Polytrodes: High-Density Silicon Electrode Arrays for Large-Scale Multiunit Recording

Timothy J. Blanche,[1] Martin A. Spacek,[1] Jamille F. Hetke,[2] and Nicholas V. Swindale[1]

[1]*Department of Ophthalmology and Visual Sciences, University of British Columbia, Vancouver, British Columbia, Canada; and*
[2]*Department of Electrical Engineering and Computer Science, University of Michigan, Ann Arbor, Michigan*

Blanche, Timothy J., Martin A. Spacek, Jamille F. Hetke, and Nicholas V. Swindale. Polytrodes: high-density silicon electrode arrays for large-scale multiunit recording. *J Neurophysiol* 93: 2987–3000, 2005. First published November 17, 2004; doi:10.1152/ jn.01023.2004. We developed a variety of 54-channel high-density silicon electrode arrays (polytrodes) designed to record from large numbers of neurons spanning millimeters of brain. In cat visual cortex, it was possible to make simultaneous recordings from >100 well-isolated neurons. Using standard clustering methods, polytrodes provide a quality of single-unit isolation that surpasses that attainable with tetrodes. Guidelines for successful in vivo recording and precise electrode positioning are described. We also describe a high-bandwidth continuous data-acquisition system designed specifically for polytrodes and an automated impedance meter for testing polytrode site integrity. Despite having smaller interconnect pitches than earlier silicon-based electrodes of this type, these polytrodes have negligible channel crosstalk, comparable reliability, and low site impedances and are capable of making high-fidelity multiunit recordings with minimal tissue damage. The relatively benign nature of planar electrode arrays is evident both histologically and in experiments where the polytrode was repeatedly advanced and retracted hundreds of microns over periods of many hours. It was possible to maintain stable recordings from active neurons adjacent to the polytrode without change in their absolute positions, neurophysiological or receptive field properties.

INTRODUCTION

Silicon-based multichannel electrode arrays (Campbell et al. 1991; Drake et al. 1988; Ensell et al. 2000; Kewley et al. 1997; Kovacs et al. 1994; Norlin et al. 2002; Spence et al. 2003; Wise and Najafi 1991; Yoon et al. 2000), or polytrodes, afford electrophysiological recording capabilities beyond those of conventional single-unit or multiple wire electrodes. As with stereotrodes (McNaughton et al. 1983) and tetrodes (Wilson and McNaughton 1993), polytrodes are designed to make extracellular multiunit recordings from adjacent active neurons. Polytrodes with closely spaced recording sites possess the improved unit isolation of tetrodes and like tetrodes can record from up to three times as many neurons as electrode sites (Gray et al. 1995; Harris et al. 2000; Hetherington and Swindale 1999; Maldonado and Gray 1996; Maldonado et al. 1997). In addition, the precise lithographic process by which polytrodes are defined ensures consistent recording properties and makes possible arbitrary electrode shapes (single or multiple shank) and configurations of recording sites tailored for specific brain structures or applications. The number and density of sites that can be etched onto a minute piece of silicon (as narrow as 15 μm wide and 1–15 μm thick) far exceeds that of wire electrodes, effectively increasing neuronal yield while minimizing tissue displacement and potential for damage. Polytrode materials are biocompatible (Niparko et al. 1989) and are suitable for chronic implantation (Hetke et al. 1994; Hoogerwerf and Wise 1994; Mensinger et al. 2000; Rousche and Normann 1998; Vetter et al. 2004), and cortical microstimulation (Anderson et al. 1989; Rousche and Normann 1999; Weiland and Anderson 2000). Polytrodes with integrated circuitry for buffering, multiplexing, amplification, and signal processing (Bai and Wise 2001; Csicsvari et al. 2003; Hoogerwerf and Wise 1994; Najafi and Wise 1986; Takahashi and Matsuo 1984) can minimize noise, channel cross-talk and movement-related artifacts in chronically implanted devices. Microma-chined fluidic channels can also be incorporated into the silicon substrate for cellular-scale chemical and neurotransmitter delivery (Chen et al. 1997; Rathnasingham et al. 2004).

This flexibility of design has allowed polytrodes to be used successfully in a diversity of applications and brain areas, from multiunit studies of neocortical plasticity (Fu et al. 2002) to hippocampal recordings in awake-behaving animals (Buzsaki et al. 1992) and from spatiotemporal mapping of auditory cortex discharges evoked by new generation cochlear-implants (Bierer and Middlebrooks 2002) to the relationship between single units and local field potential (LFP) activity during sleep (Kandel and Buzsaki 1997). Other innovative applications, such as in vivo studies of backpropagating action potentials (BPAPs) (Buzsaki and Kandel 1998), deducing intracellular parameters from extracellular waveforms (Henze et al. 2000), and three-dimensional spatial neuron localization (Blanche et al. 2003; Hetherington et al. 1999), would arguably not be possible with other contemporary electrode technologies.

Our interest in polytrodes was motivated by persistent questions in visual neurophysiology (Olshausen and Field 2004) that could only be addressed with an electrode capable of recording simultaneously from large numbers of neurons in whole cortical columns. Furthermore, to determine the precise location of recorded neurons in the cortical layers, and classification of cell type based entirely on extracellular voltage distributions, requires high-resolution spike field potential measurements. In this paper, we describe five novel high-density 54 channel polytrodes developed for these studies. We demonstrate their use, handling, and recording characteristics in acute cat visual cortex experiments. The customized hard-

ware needed to record from polytrodes is described, including personal computer-based continuous data-acquisition software, an automated impedance meter for testing recording site viability, and techniques for precise electrode positioning. We conclude by considering the sorts of neurophysiological questions polytrodes are ideally suited to explore.

METHODS

High-density polytrodes

Each of the 54-channel polytrodes described in this report (Table 1) is a single-shank planar electrode array designed for acute in vivo recordings. All are passive devices (i.e., no on-chip electronics) that were fabricated and packaged by the University of Michigan's Center for Neural Communication Technology (CNCT). The lithographic process for producing silicon substrate electrodes (Najafi et al. 1985) was pushed close to standard University of Michigan manufacturing limits by halving the usual interconnect conductor width and spacing from 3 to 1.5 μm. The overall width of the shank was dictated by the number of recording sites and associated conductors, so this refinement was necessary to keep the shank width as narrow as possible. Previous work (Drake et al. 1988) had shown that 15-μm-diam sites were ideal for high signal-to-noise ratio (S:N) multiunit recordings, so this size was adopted for these polytrodes. The other design consideration was the geometric configuration and spacing of the recording sites. We experimented with a number of co-linear and staggered site arrangements with different inter-site spacing (Fig. 1A) to achieve a good trade-off between adequate sampling and isolation of individual neurons (which requires spikes to appear on multiple sites), and traversal of as much brain as possible with a finite number of sites. Each configuration has specific advantages. The polytrode with the most closely spaced sites was designed to make high-resolution measurements of spike field potentials, with individual spikes appearing on ≥12 sites. Data derived from this polytrode were needed to "bootstrap" a quantitative field potential model for three-dimensional (3D) spatial neuron localization and classification of cell type (Blanche et al. 2003). The two-column staggered polytrodes were designed to maintain good single-unit isolation yet be sufficiently long to record from all layers in a cortical column, whereas the hexagonal three-column designs were a compromise of both these needs.

The polytrodes were ultrasonically bonded to a custom-made, commercially available (Neuralynx, Tuscon, AZ) printed circuit board (Fig. 1B). Each polytrode incorporates additional silicon substrate (4–5 mm) interposed between the recording sites and the bond pads to allow it to be inserted into the craniotomy cavity without obstruction from the skull. The interface board supports the headstage preamplifiers in close proximity to the polytrode, thereby minimizing electrical and radio-frequency interference. It also serves as a point of attachment for the electrode holder and provides electrical access to recording sites for cortical microstimulation, cortical lesioning, or electrolytic track marking.

Ready-bonded polytrodes of various designs, including those described here, are now commercially available from NeuroNexus Technologies (http://www.neuronexustech.com).

Polytrode site impedance tester

Prior to an experiment it was important to identify any faulty recording sites that were shorted together or electrically open. If open "floating" sites were not grounded, they tended to either saturate the amplifiers, producing noise on adjacent functional channels, or else exhibited spurious spike-like signals by capacitively coupling to adjacent conductors. Manually testing every site is laborious and error prone, so an automated multichannel site impedance tester was custom-made specifically for this purpose. The device utilizes software-controlled analog multiplexers to automate switching between recording sites and is able to test an entire 54-channel polytrode in less than a minute. An on-line graphical display provides a report of impedance magnitude and phase for each site, highlighting any open or shorted sites. The basic circuit schematic (Fig. A1) and operational details are described in the APPENDIX. Unless otherwise stated, all impedance measurements were made in 0.9% phosphate-buffered saline (PBS) against a large saturated calomel reference electrode (Accumet No. 13 620 52).

The possibility that the closer spacing and narrower conductor widths of these polytrodes might make them susceptible to excessive channel cross-talk was tested by injecting a 100-μVrms, 1-kHz sine wave into individual electrode sites via the electrode interface board. The polytrode tip was immersed in PBS with a common reference electrode in the saline. Evidence of capacitive coupling in adjacent nonsignal channels was looked for in the edge-triggered average of a few hundred cycles of the test signal.

Surgery and recording procedures

Adult cats or rats were prepared for acute electrophysiological recordings in accordance with guidelines established by the Canadian Council for Animal Care. For the initial surgery, cats were anesthetized with an intravenous bolus of sodium thiopental (2.5% wt/vol) to effect, with booster injections administered as needed. Either intubation or a tracheotomy was performed, and the cat was placed in a stereotaxic frame and connected to temperature, blood pressure, electrocardiograph (ECG), electroencephalograph, pO_2, and end-tidal CO_2 monitors. Pressure points and wounds were infiltrated with the local anesthetics lidocaine (10%) and bupivacaine hydrochloride (Marcaine, 0.25%), respectively. Dexamethasone (0.3 mg im) was given to prevent brain edema. Intravenous injections of anesthetics were discontinued, and surgical anesthesia was maintained by artificial ventilation with a mixture of 70% N_2O and 0.25–1.5% isoflurane in oxygen. Core body temperature was maintained near 38°C with a thermostatically controlled heating pad, and end-tidal $SpCO_2$ and pO_2 were stabilized at 40 mmHg and 99–100%, respectively, by varying the respiration rate. A 5 × 10-mm craniotomy was made over cortical areas 17 and 18. With the aid of a surgical microscope, a small area of dura was carefully reflected. At this point paralysis was induced with pancuronium bromide (2 mg/kg) and maintained throughout the experiment by continuous intravenous infusion of pancuronium (0.2 mg · kg^{-1} · h^{-1}) dissolved in lactated Ringer with 5% dextrose, delivered at a rate of 3 ml · kg^{-1} · h^{-1}. Pupils were dilated with topical atropine (5%), and nictitating membranes were retracted with phenylephrine eye drops (10%). Reverse ophthalmoscopy was used to choose rigid gas-permeable contact lenses (Harbour City Contact Lens Services, Nanaimo, BC, Canada) of appropriate radius of curvature and power to focus both eyes on the stimulus display monitor positioned 50 cm in front of the cat. Additional drops of phenylephrine and atropine were applied as needed.

TABLE 1. *Polytrode specifications*

Polytrode Design	Site Configuration	Site Spacing, μm	Extent, μm*	Recording Span, μm†
54μmap1a	3 column, hexagonal	65	1138	1400
54μmap1b	3 column, collinear	50$_v$/46$_h$	850	1100
54μmap1c	3 column hexagonal	75	1313	1600
54μmap2a	2 column, staggered	65	1723	2000
54μmap2b	2 column, staggered	50	1325	1600

Comparison of the five polytrodes used in this study. Each has 54 recording sites distributed in a variety of configurations and inter-site spacings. *, distance between the most vertically disparate sites. †, approximate distance along the long axis of the polytrode over which neurons can be recorded, assuming isolatable units are recordable up to ~150 μm beyond the top and bottom recording sites (Blanche et al. 2003).
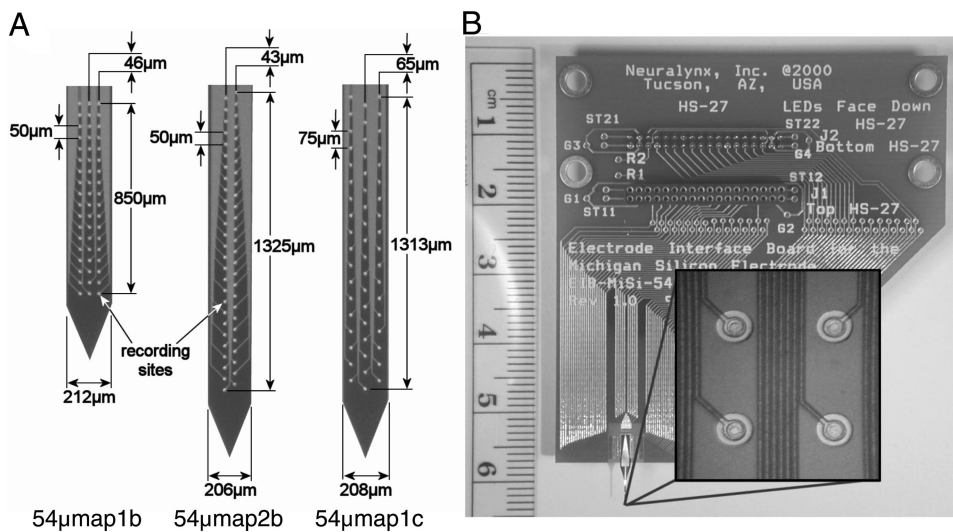
FIG. 1. Fifty-four site polytrodes. *A*: photomicrographs of 3 of the 5 polytrode designs. The polytrode shanks have planar recording sites spaced 43–75 μm apart in 2 or 3 columns. Polytrodes with denser site spacing (*54μmap1b*) provide highly detailed field recordings, and span ~1 mm. The longer 2 column polytrodes (*54μmap2b*) traverse 1.3~1.7 mm, enabling simultaneous recordings of units from entire cortical columns in cat visual cortex. Another design (*54μmap1c*) has a slightly larger intersite spacing in a hexagonal array, and spans ~1.3 mm (dimensions for all polytrode designs are given in Table 1). *B*: A 54μmap1b polytrode, shown here bonded to the headstage interface board, has closely spaced co-linear sites arranged in 3 columns. The slightly raised (0.3 μm) recording sites and associated interconnects are visible (*inset*). All shanks are 15-μm thick, 199–212 μm wide (depending on the design), with 15-μm diam iridium recording sites.

Adult rats were anesthetized with ketamine/xylazine (50/10 mg/kg ip) and placed in a rodent stereotaxic frame. A small craniotomy/durotomy was made over the visual areas of one hemisphere. Vital signs including ECG, pO_2, and core temperature were monitored throughout the procedure, the latter regulated with a small DC heating pad.

Polytrodes are extremely flexible and cannot penetrate the *dura mater* without fracturing, nor usually the *pia mater* without excessive dimpling of the brain. It was thus necessary to reflect the dura and make a tiny incision (~300 μm long) in the pia using ultra-fine micro-dissection scissors (Fine Science Tools, Vancouver, BC, Canada) or a 32-gauge needle bent at the end to create a micro-sized hook. Alternatively, angled slit knives intended for ophthalmic microsurgery (ClearCut 3.2 mm, Alcon Surgical) were also ideal for opening the pia. The polytrode could then be inserted without bending or dimpling of the brain. Tight physical and electrical coupling of the recording sites to the cortical tissue is essential for robust recordings (Starr et al. 1973). We suspect that fluid on the surface of the brain, if allowed to seep down between the silicon substrate and neuropil, acts as a low-impedance shunt to ground, heavily attenuating or even abolishing spike amplitudes. For this reason, we routinely wicked away any cerebrospinal fluid (CSF) during insertion. While viewing the exposed surface of the brain through a surgical microscope, the polytrode was slowly advanced into the cortex with a micromanipulator (Narishige MHW-4, East Meadow NY) until the top sites were ~200 μm below the surface. The usual practice was to record at a single fixed position per penetration, either traversing a cortical column by inserting vertically in the crown of the lateral gyrus, or down the medial bank of the lateral gyrus for *trans*-columnar recordings. Only when addressing specific technical questions relating to neuronal damage and stability of unit isolation was the polytrode repeatedly advanced and retracted. After insertion the craniotomy was filled with agar (2.5% in artificial CSF) to diminish brain movements.

Spike amplitudes were often attenuated or even abolished after advancement or retraction of the polytrode, presumably due to loss of electrical coupling. For this reason, we routinely waited for at least half an hour for the polytrode position to stabilize and recouple to the tissue. During this period, spike amplitudes were usually restored.

Spikes were evoked with a wide range of visual stimuli, including drifting bars and sinusoidal gratings, white, pink, and m-sequence noise, flashed stimuli, and natural scene movies. Stimuli were presented on a display monitor (Sony 200sf) with a 100-Hz refresh rate and software-linearized gamma correction (mean luminance: 55 cd/m^2). All data presented here were recorded from cortical neurons in primary visual areas 17 and 18.

Recordings in cat were typically made for 3–8 h in each penetration. At the completion of each recording, the polytrode tip was carefully withdrawn and immediately cleaned with a jet of de-ionized water from a squirt bottle. Long-term storage was in air. Polytrodes used for acute experiments and cleaned in this way were successfully re-used more than once. We assessed the reusability of the polytrodes by monitoring site impedances and recording performance in successive experiments over several years.

Instrumentation and acquisition software

The electrophysiology system was assembled from commercially available and custom-built hardware. Extracellular electrical activity, referenced to a platinum wire loop positioned around the craniotomy, was buffered by two 27-channel unity-gain headstage preamplifiers (HS-27s, Neuralynx) prior to amplification with a 64-channel amplifier (Multichannel Systems FA-I-64, ALA Scientific Instruments, Westbury, NY). The amplifier channels had a factory-fixed gain of 5,000, 54 of which were band-pass-filtered for recording units (500–6 kHz), the remaining 10 for recording LFPs (0.1–150 Hz). A custom-made patch box (Multichannel Systems) enabled a selection of the polytrode sites to be passed to the LFP channels. The patch box also relayed power to the headstage preamplifiers and was used as a grounding point for any faulty polytrode sites. Prior to sampling signals were further amplified two to eight times (A/D converter ranges from ± 1 to ± 250 μV full-scale) and digitized with 12-bit resolution by two synchronized 32-channel acquisition cards (DT3010s, Data Translation, Marlboro, MA) at 25 kHz/channel.

During recording, waveform and stimulus display-related data were displayed on-line and continuously streamed to hard disk using in-house software. Spike waveforms were displayed in one millisecond epochs in the same layout as the recording sites to provide a meaningful display of activity across the polytrode (Fig. 2). The software is preprogrammed with the site configurations of the five polytrodes described in this report (Table 1), in addition to other 16-channel polytrodes made by the CNCT. It can accommodate an arbitrary number of polytrodes, tetrodes, and single-channel electrodes, treating each as a separate entity with respect to gain, sample rate, and display. Knowledge of the precise geometry of recording sites was used throughout subsequent stages of spike detection and sorting (Spacek et al. 2003), and physiological analyses (Blanche et al. 2003).

LFP and EEG signals were viewable on chart-like scrolling displays, and the one-dimensional current source density (CSD) profile derived from the LFPs provided on-line feedback of the depth and
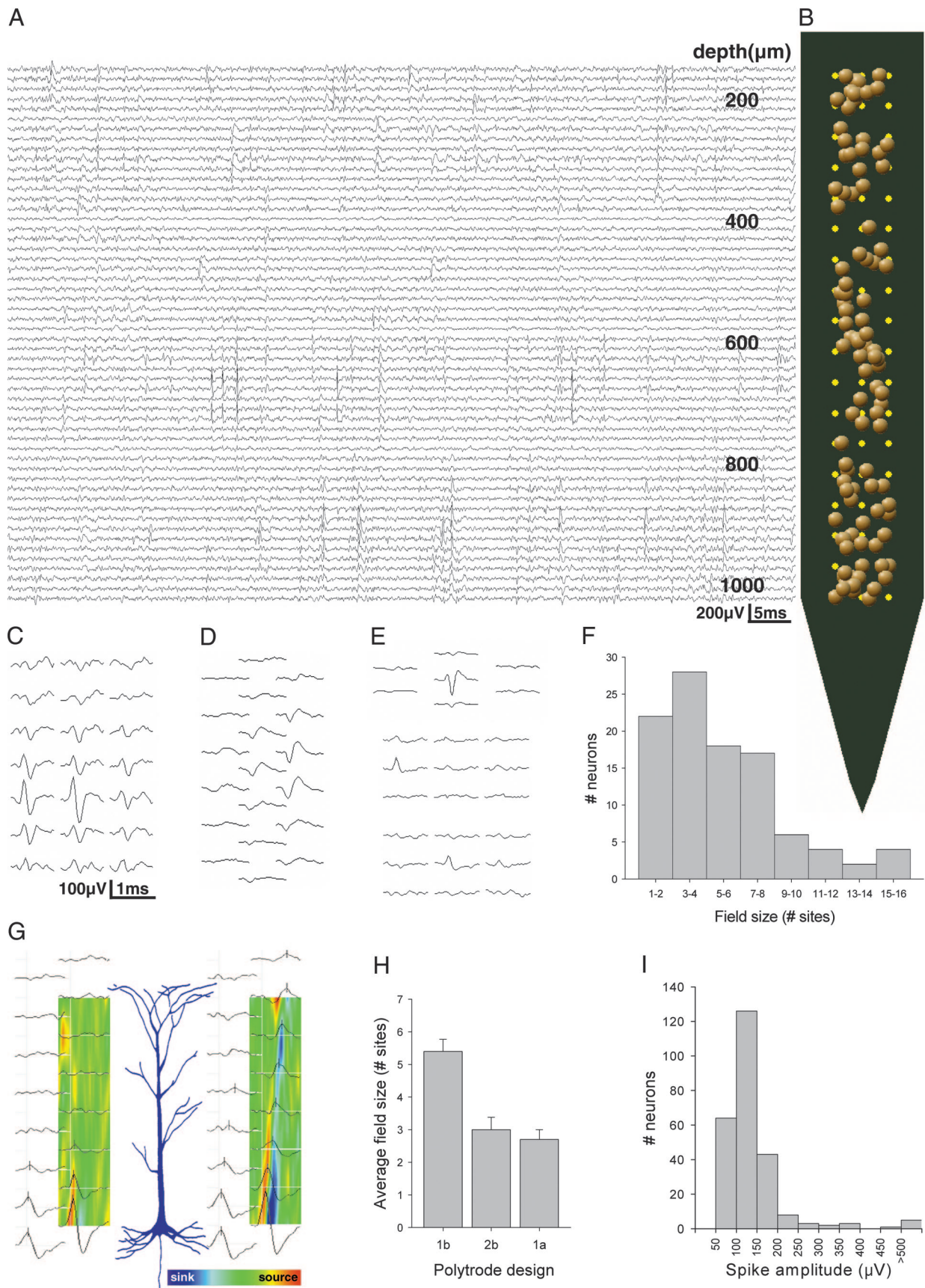
alignment of the polytrode in relation to the cortical laminae (see following text). The software also displayed EEG spectrograms to monitor brain state and depth of anesthesia. The use of an optimized compiler (Delphi, Borland), low-level assembler code where appropriate, and PCI bus-mastered transfer of waveform signals make the system efficient and scalable (64 channels used ~10% CPU load on an AMD Athlon 1800+). In practice, the number of channels is thus only limited by the number of amplifiers and acquisition cards installed. Data were losslessly compressed and archived on 4.7 GB DVDs.

On-line CSD analysis

Generalized activation of the optic pathway via direct thalamic or photic stimulation evokes a characteristic laminar activation pattern in the primary visual cortex that can be revealed by CSD analysis (Mitzdorf and Singer 1978). Although CSD analysis is a legitimate electrophysiological tool in its own right (e.g., Mitzdorf 1985), it is exploited here solely to determine the depth of the polytrode in the cortical laminae. Evoked responses to brief flashed stimuli (full frame, 10-ms duration) are averaged, and the one-dimensional CSD is computed from the second spatial derivative of LFPs on vertically aligned (translaminar) sites

$$\frac{\delta^2 \phi}{\delta z^2} \approx \frac{\phi_{(z+n\Delta z)} - 2\phi_{(z)} + \phi_{(z-n\Delta z)}}{(n\Delta z)^2} \text{ (Nicholson and Freeman 1975)}$$

where ϕ is the average evoked field potential, z is the electrode site coordinate perpendicular to the layers, Δz is the sampling interval (100–150 μm depending on the polytrode), and $n\Delta z$ is the differentiation grid (typically $n = 2$).

The differentiation grid is equivalent to spatial smoothing and reduces high spatial frequency noise. To aid visualization of the CSD profile, color-mapped time series were generated using cubic spline interpolation (Press et al. 1994) along the depth axis.

Acute histological procedures

To determine more precisely the position of the polytrode in the cortex, acute histological procedures were established that avoid tissue shrinkage usually associated with fixatives. These methods were developed and tested in rat for use in the cat experiments, but are equally applicable to track identification in other species. They provide an independent validation of polytrode depth obtained from CSD measurements.

Prior to insertion, the rear of a polytrode shank (side opposite the recording sites) was painted with fluorescent 1,1′-dioctadecyl-3,3,3′,3′- tetramethylindocarbocyanine perchlorate (diI, ~10% in ethanol, Molecular Probes, Eugene, OR) (DiCarlo et al. 1996). As this dye is a lipophilic neuronal tracer, uptake into adjacent neurons and processes also allowed assessment of the level of structural damage caused by the polytrode. The recording properties of the polytrode did not appear to be affected by the dye. The polytrode was inserted into the cortex so that the top row of electrode sites was ~200 μm below

the surface of the brain. CSD profiles were evoked by photic stimulation and saved to file for later registration with the histology.

Immediately posteuthanasia the cortical region of interest was blocked in situ, removed, and bathed in chilled PBS. After carefully removing the pia mater, 300- to 400-μm-thick coronal sections were cut on a tissue vibratome and counterstained with green fluorescent Nissl stain (Neurotrace 500/525, Molecular Probes). Nissl substance is abundant in the rough endoplasmic reticulum of neuronal cells, and Neurotrace is the fluorescent analog of traditional chromophoric Nissl stains such as cresyl violet. Briefly, the counterstain procedure involved permeabilizing the tissue with Triton X-100 (0.1% wt/vol in PBS) for 10 min, followed by two 5-min washes with PBS. The brain slices were incubated for 30 min in a 50-fold dilution of the supplied stock solution. After repeating the permeabilization and washing steps, the slices were transferred to glass slides with 90% wt/vol glycerol + DABCO (an antifade agent) in PBS and coverslipped. The polytrode track, clearly demarcated by the diI against the Nissl-stained cortex, was then visualized on either a standard wide field or confocal fluorescent microscope (Zeiss LSM-510, Göttingen, Germany).

The degree of structural damage to the neural tissue surrounding the polytrode was further investigated in the same series of rat experiments. Instead of diI, a polytrode coated with propidium iodide (PI, ~10% wt/vol in dH₂O, Molecular Probes) was inserted into the cortex. PI is a nontoxic polar compound that can be used as an indicator of cell membrane integrity and viability (Vornov et al. 1991). The dye enters damaged or necrotic cells with leaky or otherwise compromised cell membranes, binds to nucleic acids and becomes brightly red fluorescent. After an hour the polytrode was removed, and as before 400-μm-thick coronal slices were cut from the fresh, unfixed brain tissue. The brain slices were counterstained with green fluorescent Nissl stain, mounted, and coverslipped as previously described. Neurons surrounding the polytrode track were then reconstructed from serial optical sections imaged with the confocal microscope. An objective quantification of the extent of cellular damage was made by counting the proportion of Nissl-stained cells (predominantly neurons, in green), to Nissl-stained cells co-localized with PI (damaged neurons, in yellow), to PI-positive cells (nonneuronal cells, in red).

RESULTS

General recording properties

Recording site impedances were 1.17 MΩ ± 150 kΩ at 1 kHz ($n = 1,003$, ± stdev, from 20 assorted polytrodes), with average phase angles of $-75.8 \pm 3.4°$ (i.e., largely capacitive). Such minor variations in site impedance had no measurable effect on the sensitivity of the site nor the amplitude of recorded spikes. However, sites with significantly higher impedance tended to be slightly noisier. On average individual polytrodes had 3.9 faulty sites (median 4, range 0–8), which were usually open circuit but occasionally shorted together. Exclusion of this number of faulty sites did not significantly

FIG. 2. Simultaneous recording of neuron ensembles in cat primary visual cortex. *A*: 100-ms segment of multiunit activity from a 54μmap1b polytrode (Table 1) inserted perpendicular to the surface of the cortex, traversing the cortical depth indicated. This particular recording comprised >100 spontaneously active and visually responsive neurons distributed across the length of the polytrode. Individual action potentials spanned several sites. *B*: approximate neuron positions from the same recording. The relative positions were estimated from the mean weighted spike amplitudes across channels. Diverse spike waveforms, arranged according to site layouts, recorded with (*C*) a 54μmap1b polytrode, showing a triphasic spike across 12 sites; (*D*): a 54μmap1a polytrode, with a biphasic spike on 5 of the more widely separated sites; (*E*): 3 small field, fast-spiking neurons, and a 54μmap2a polytrode (*F*) histogram showing the approximate electric field spread of the neurons recorded in *B*, defined as the number of sites with spike waveforms exceeding 50 μV$_{pp}$. Regular somatic action potentials (*left*) were typically restricted to sites within a ~150-μm radius of the maximum amplitude site (presumed to be adjacent to the axon hillock) and had instantaneous peak times (vertical dashes). In contrast, presumed back-propagating action potentials (*right*) had current dipoles (colored CSD maps) traveling 500 μm up the apical dendrite, with increasing latency to peak amplitude. *G*: showing a putative layer-5 pyramidal cell with 2 distinct spatial distributions. *H*: comparison of the average number of sites per neuron for different site configurations (see Table 1). Error bars are SE. *I*: distribution of peak-channel spike amplitudes from multiple penetrations.

compromise recordings because of the high spatial sampling of these polytrodes. In the multiunit band-pass (500 Hz–6 kHz), noise was typically 3–4 μV_{rms} (20–30 μV_{pp}), depending on the site, measured in saline. Noise in the LFP/EEG band-pass (0.1–150 Hz) was also ~3μV_{rms}, predominantly 60-Hz line interference. All designs had negligible channel cross-talk. Even channels with adjacent interconnects showed <0.5% coupling. Taken together, the consistency of recording site properties indicates that the fabrication process for these polytrodes was as reliable as that for "standard" 16 channel polytrodes (Najafi et al. 1985), despite smaller feature sizes and higher site densities.

Representative multiunit recordings are shown in Fig. 2. In a sample of 255 neurons from eight penetrations (Fig. 2I), spike amplitudes ranged from noise up to 1.2 mV_{pp} (mean 144 ± 118 μV), presumably due to differences in the size, morphology and proximity of the neuron to the electrode sites (Bishop et al. 1962a,b; Drake et al. 1988; Fatt 1957; Henze et al. 2000; Humphrey 1976; Rosenthal et al. 1966). Given an aggregate noise level of 30–40 μV_{pp} (including thermal and biological noise from distant neuronal activity), this translates into a S:N of up to 30:1. For the majority of recorded neurons with peak-channel spike amplitudes of ~130 μV_{pp}, a 4:1 ratio was attained, more than adequate for spike sorting. These amplitudes are comparable to those recorded extracellularly with conventional multiunit electrodes and tetrodes (Gray et al. 1995; Hetherington and Swindale 1999). Given the similar impedances and surface area of recording sites, this result was expected but not guaranteed because polytrodes comprising planar electrode sites only record neurons in front of the insulating shank (Drake et al. 1988) not around the vicinity of the tip (Henze et al. 2000).

As with any electrophysiological recording, neuronal yield is determined by many factors, including the number of nearby active neurons, depth and type of anesthesia, type of visual stimulation, and cortical location (e.g., granular vs. agranular layers). Identification of well-isolated single units is also dependent on good S:N and the efficacy of spike detection and sorting. Our experimental conditions (acute recordings in anesthetized cat visual cortex) routinely yielded between 20 and 50 isolatable units recorded simultaneously at a given location. One of the best recordings in our database contains >100 clearly distinct neurons (Fig. 2A), recorded at a single position and isolated using multichannel template-based clustering procedures (Spacek et al. 2003; unpublished data). Active neurons were distributed along the full extent of the polytrode (Fig. 2B).

With respect to field potential spread, on the highest density three-column polytrode (1b design) up to 16 sites detected the action potentials from (presumed) pyramidal neurons with large "open" fields (Fig. 2, C and G). Individual spikes on the polytrode with sites spaced 65 μm apart in a hexagonal layout (1a design) were recorded by up to 9 sites (Fig. 2D). Fast spikes from smaller "closed-field" neurons, most likely interneurons (Bartho et al. 2004; Blanche et al. 2003; Henze et al. 2000; Humphrey 1976), showed appreciable signal on only one or two sites irrespective of the intersite spacing (Fig. 2E). In contrast, some neurons infrequently discharged spikes with current dipoles moving hundreds of micrometers (Fig. 2G),

with a velocity (0.7 ± 0.15m/s) and direction consistent with a BPAP traveling up the apical dendrite (Buzsaki and Kandel 1998; Johnston et al. 1996).

Improved single-unit isolation

To compare the multiunit recording performance of these polytrodes against more established techniques, we constructed "virtual tetrodes" (all sets of 4 adjacent polytrode sites excluding faulty ones) from the 54μmap1b recording shown in Fig. 2A. This polytrode has a site spacing comparable to that of real wire tetrodes (Jog et al. 2002). Including any neuron with a spike amplitude >60 μV_{pp} on at least one channel of each virtual tetrode, we counted between 7 and 24 neurons per tetrode (mean = 17.1 ± 4, n = 101), roughly double that typically reported for wire tetrodes (Gray et al. 1995; Harris et al. 2000; Hetherington and Swindale 1999; Maldonado and Gray 1996; Maldonado et al. 1997). Virtual tetrodes with ≥10 neurons were common in other recordings, which raises an important question: in a real tetrode recording, how many neurons identified as single units are actually multiple neurons? A case study addressing this issue is presented in Fig. 3. In this example, 10 neurons were identified on a virtual tetrode (Fig. 3A) using multichannel template-based clustering (Spacek et al. 2003), and the first two principal components (PCs) derived from these templates were used to manually or automatically [Klustakwik (Harris et al. 2000)] cluster the data. The Mahalanobis distance (Mahalanobis 1936) was used to quantify the distance d_{ij} between the centroids of any cluster pair $x_i = (x_1 \ldots x_n)$ and $y_1 = (y_1 \ldots y_n)$ in n-dimensional feature space

$$d_{ij} = \sqrt{(x_i - y_j)^T C^{-1}(x_i - y_j)}, \; S = \bar{d}_{ij} \quad \text{for} \quad i,j = 1 \ldots N, \; i \neq j$$

where C is the covariance matrix of the cluster pair, S is the average cluster pair separation, and N is the number of clusters. Both clustering methods could separate seven of the neurons using the tetrode-derived PCs ($S = 14.5$), but neither method was able to separate the three other neurons ($S = 3.7$) due to the close similarity of their waveforms on the tetrode sites (Fig. 3B). However, when the PCs from the surrounding polytrode sites were included (Fig. 3C), both clustering methods accurately separated the three neurons ($S = 12.1$), and the separation of the other seven neurons ($S = 16.3$) also improved. So an actual tetrode positioned at this location would have produced eight clusters; seven that represented valid single units, and an eighth supercluster comprised of three neurons, indistinguishable from a valid single-unit cluster, except perhaps by other criteria (e.g., an autocorrelogram without a 1-ms refractory period, although this test is unsuitable for fast spiking neurons (Nowak et al. 2003)).

Polytrode reusability

Polytrode site impedances were measured after long-term storage and repeated use in acute 3- to 5-day experiments run several months apart (Fig. 4A). Although there was a slight increase in average site impedances from 1.1 to 1.3 MΩ, this was without concomitant deterioration of recording performance. The number of faulty sites did not increase, and neuronal yield and spike amplitudes remained qualitatively unchanged. Inert iridium recording sites, when
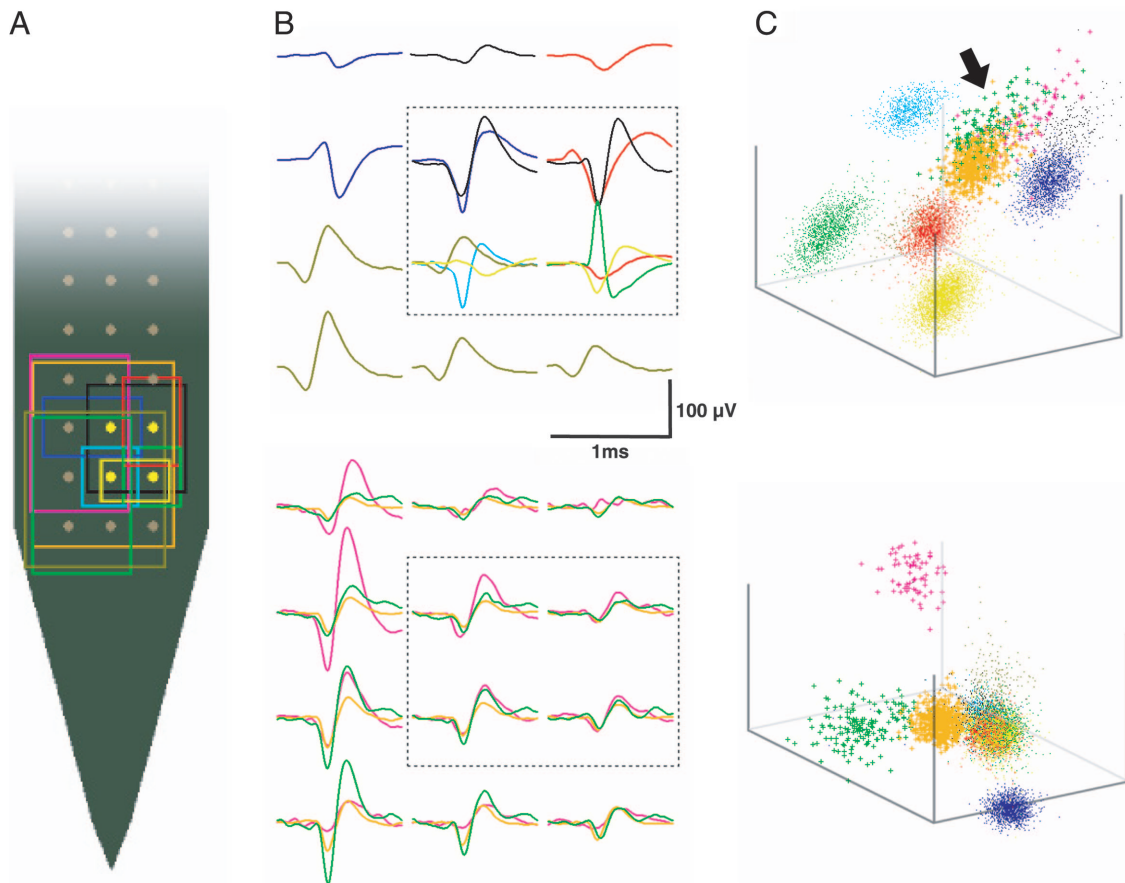
FIG. 3. Polytrodes provide better single-unit isolation than tetrodes. *A*: breaking the polytrode into "virtual tetrodes" revealed that 7–24 neurons were recorded on any one virtual tetrode of a 54μmap1b polytrode. In the example shown here (highlighted sites), 10 neurons were identified, their approximate field sizes represented by the colored boxes. *B*: spike waveforms of these 10 neurons, 7 of which were isolatable using the tetrode sites alone (*top boxed region*) and 3 that could only be isolated by including spike waveforms from the surrounding recording sites (*bottom*). Note the similarity of the spike shapes and amplitudes on the tetrode sites. *C*: a tetrode-derived cluster plot (*top*) shows 5 of the 7 well-isolated neurons. Whereas 2 other neurons (black and gold dots) were separable along other dimensions, 3 neurons (arrow: green, orange, and pink + symbols) were not distinguishable on any projection or hyperplane of the tetrode. Only by incorporating spike waveform indices from the surrounding sites was it possible to cluster and isolate these neurons (*bottom*).

washed immediately after use and stored in air, can thus be repeatedly re-used for hundreds of hours under these conditions. Our polytrodes are eventually broken during handling, but we have yet to discard any due to degradation of site impedances or recording characteristics. Site imped-

ances can be restored to preuse levels by soaking the polytrode tip overnight in 0.25% wt/vol trypsin-EDTA (Invitrogen), followed by thorough rinsing in distilled water (Fig. 4*B*). Most accumulated proteinaceous material is removed by this simple cleaning procedure.
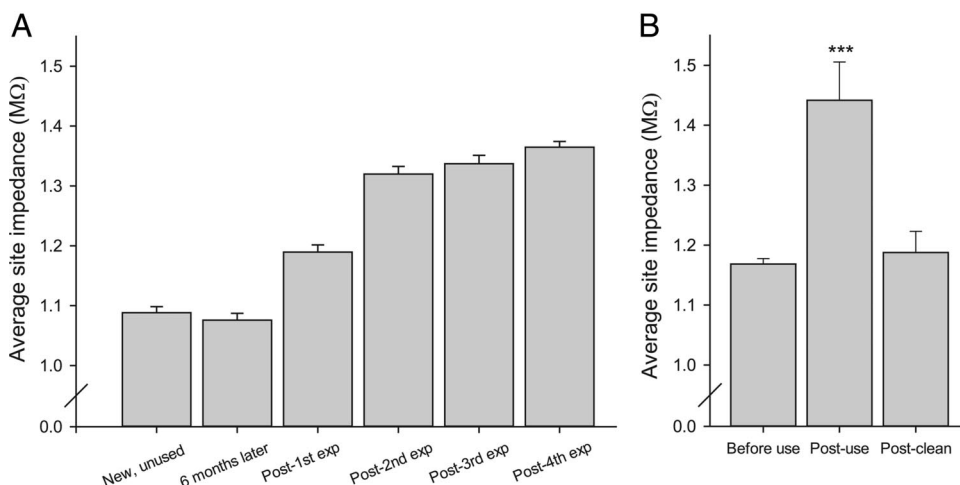

FIG. 4. Long-term stability of recording sites. *A*: post fabrication site impedances were highly consistent and remained unchanged for 6 mo when stored in air. Over the course of several cat experiments with multiple penetrations in each experiment, site impedances increased slightly; however, recording properties remained similar. *B*: site impedances of another polytrode, before use, after 5 recording sessions, and after overnight cleaning in trypsin (***$P < 0.0005$). Error bars are SE.

Track reconstruction and assessment of tissue damage

Without direct staining or electrolytic lesions, it is difficult to discern polytrode penetrations in histological sections. This is encouraging from the perspective of tissue displacement, but an obstacle for determining the location of recorded cells. The diI track staining method (Fig. 5), is a straightforward and effective way of determining polytrode depth and alignment, avoiding the confound of tissue shrinkage associated with histological processing. Because the position of the recording sites on the polytrode shank is known, it is possible to infer the precise cortical location of every site by simply imaging the outline of the polytrode (Fig. 5, *A* and *E*). CSD analysis (Fig. 6) provides a complementary measure of polytrode depth.

Regarding polytrode-induced tissue damage, we found no evidence of extensive tearing or distortion of neurites or pericytes (Fig. 5*B*). The track was ~20 μm thick, and surrounding microvasculature appeared undamaged (Fig. 5*C*). Neuronal somata immediately around the track had ostensibly normal morphologies (Fig. 5*D*). Staining with PI showed that damaged neurons and glia were restricted to a region immediately surrounding the penetration (Fig. 7*A*). The percentage of

damaged neurons decreased exponentially with distance from the polytrode (Fig. 7, *C* and *D*). Of the total recordable volume in front of the polytrode (0.0126 mm^3 for the field of view shown in Fig. 7*B*), <2% of the neurons were damaged or necrotic. It is important to emphasize that this is likely an overestimate of the neuronal damage. Some of the Nissl stained cells were probably glia, and staining for PI does not necessarily indicate cell death, only that an axon or dendrite had been sufficiently compromised to permit uptake of the dye.

We found no indication of any difference in the prevalence, quality, or amplitude of neurons recorded at the top, bottom, or central recording sites. For example, in the recording portrayed in Fig. 2*B*, there were 32, 36, and 33 neurons distributed on the top, middle, and bottom recording sites, respectively. On numerous occasions, we have been able to monitor and record neuron ensembles over successive advancements of the polytrode over hundreds of micrometers for many hours. Moreover, the same neurons—as determined by their spike shapes and field potential distributions across the polytrode, relative spatial locations, firing patterns, and distinctive receptive field properties—can be recorded on *retraction* of the polytrode, without noticeable deterioration of these properties (Fig. 8). Together with the histological results, it is reasonable to
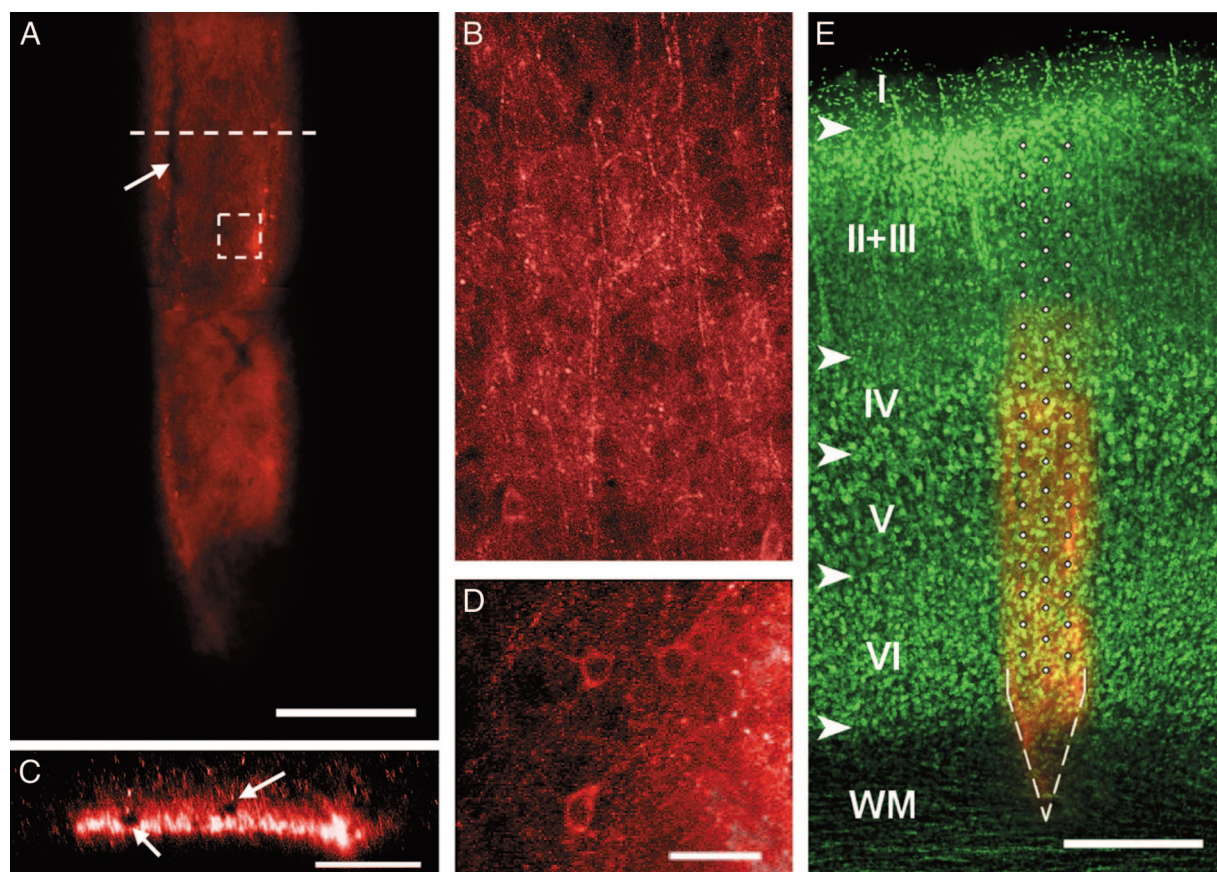

FIG. 5. Histological track reconstruction. *A*: a coronal rat brain section stained with fluorescent diI deposited by the polytrode, showing the faint outline of the tapered tip. A blood vessel (arrow) is visible running along the plane of the track. Scale bar = 200 μm. *B*: reconstruction of a 50-μm stack of confocal images directly in front of the penetration. Stained processes are neurites and pericytes indicative of normal tissue morphology. *C*: cross-section of the polytrode track at the level of the - - - in *A*. The thickness of the track is indicated by the region of intense diI fluorescence. Note the proximity of the intact microvessels (arrows). Scale bar = 75 μm. *D*: enlarged single plane confocal image 15 μm anterior to the penetration site (boxed region in *A*), shows 3 neurons and their processes. Scale bar = 50 μm. *E*: the same electrode penetration, counterstained with fluorescent Nissl stain to delineate the boundaries of the cortical layers (arrows). Because the depth and orientation of the polytrode is clearly defined tip outlined, (----), the lamina location of the electrode sites can be precisely determined (white circles). The faded region in the top right-hand corner was caused by photobleaching during earlier high-power imaging. Scale bar = 300 μm.
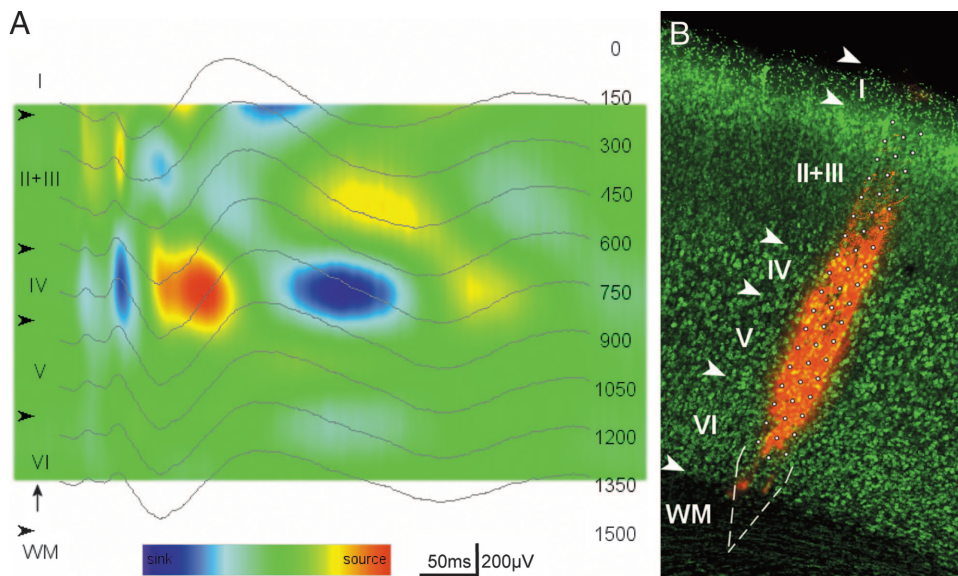
FIG. 6. CSD analysis. *A*: photic stimulation evokes characteristic local field potential (LFP) responses in rat visual cortex ($n = 400$, average traces), from which a current source density (CSD) profile was derived (color map). Prominent current sinks and sources in upper layer II/III and IV can be used to identify the depth of the polytrode with respect to the cortical layers (*arrows*). In this example the top and bottom polytrode sites were 150 and 1350 μm deep, respectively (cortical depth in μm is indicated on the right of the figure). The flash (vertical arrow) duration was 10 ms, LFPs were sampled (Δz) every 150 μm, and for the differentiation grid $n = 2$. *B*: histological reconstruction of the electrode track confirmed the vertical alignment and depth of the polytrode (the tip was visible in the white matter of the adjacent brain section).

conclude that tissue damage caused by the polytrode is restricted and relatively minimal compared with conventional electrodes. We suggest this is because polytrodes have an ultra-thin silicon substrate (typically 15 μm) that, unlike tungsten in glass or tetrode wire bundles, does not create a bore hole as it penetrates the brain (Fig. 5*C*).

DISCUSSION

Large-scale recording of neuronal activity in the intact brain is considered by many to be a prerequisite for understanding the distributed coding mechanisms that underlie sensory-motor integration, perceptual abilities, learning, memory, and ultimately the neuronal basis of language and higher cognition
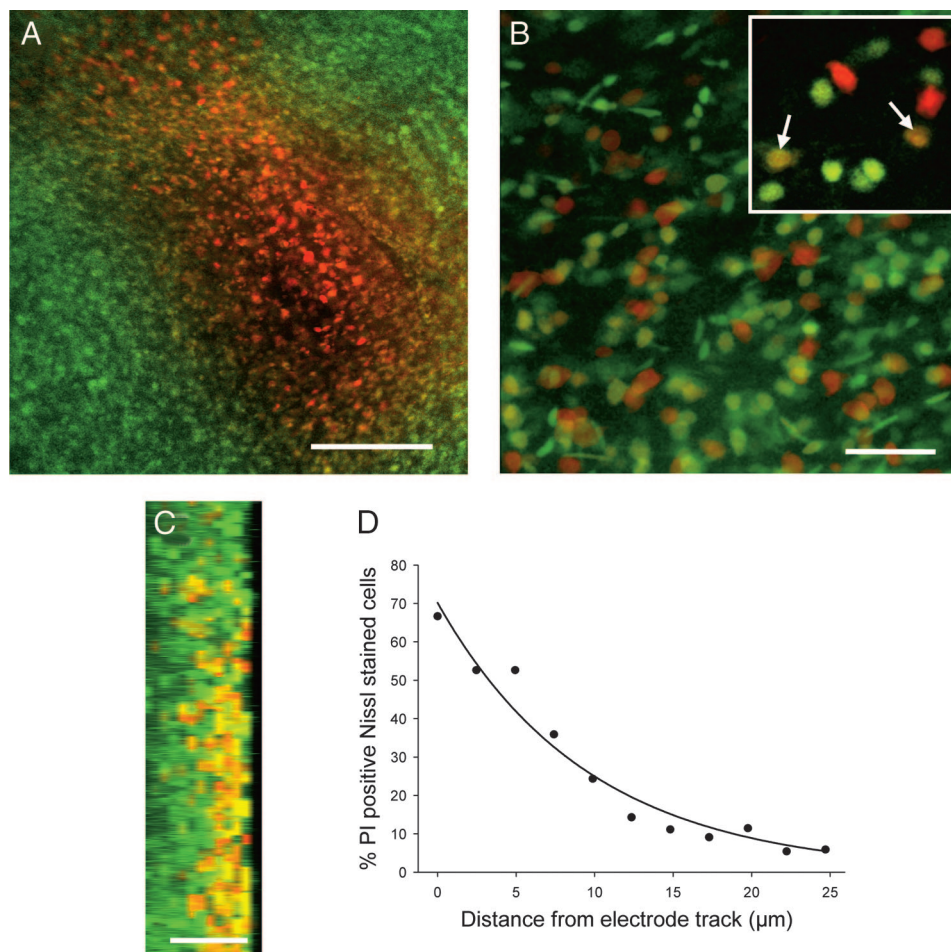

FIG. 7. Estimating neuronal damage. *A*: low power photomicrograph illustrating that PI-positive (PI+ve) cells are restricted to the vicinity immediately surrounding the polytrode. Scale bar = 150 μm. *B*: confocal reconstruction, 30 μm thick, imaged directly in front of the polytrode track. *Inset*: green fluorescent cells are undamaged neurons (including some glia), yellow cells are predominantly PI+ve damaged neurons (arrows), and red cells are PI+ve nonneuronal cells. Scale bar = 50 μm. *C*: a rotated projection of the field of view in *B* shows the limited extent of PI+ve cells with compromised membranes. Scale bar = 25 μm. *D*: the percentage of PI+ve Nissl-stained cells decreased exponentially (fitted line, $r^2 = 0.96$) with distance from the polytrode track.
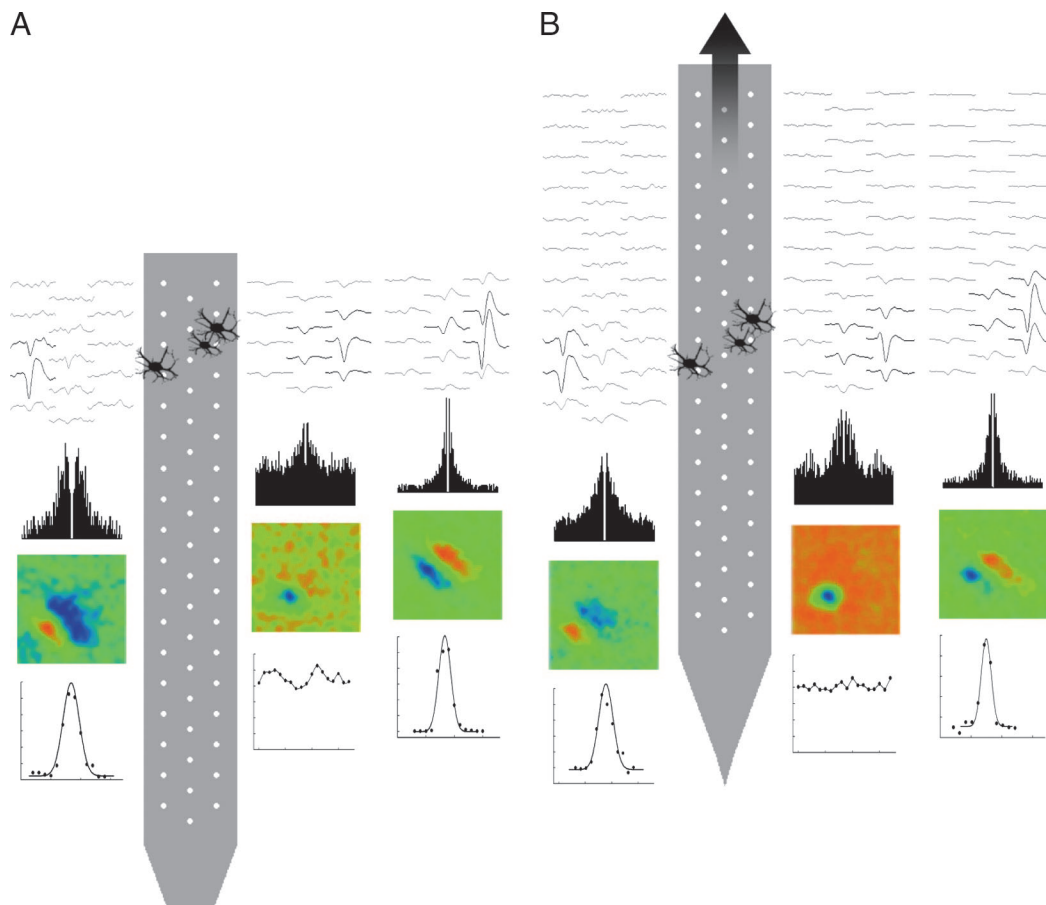
FIG. 8. Neuron passage study. An ensemble of active neurons were recorded at the point of insertion (*A*), traversing cortical layers IV–VI, and after retraction of the polytrode 400 μm (*B*; layers II/III-V), 4 h later. Averaged spike waveform epochs from 3 (of 24) visually responsive neurons are shown at both positions. Although the neurons were recorded on different sites, note the close similarity of the spike shapes and distributions. Estimated neuron locations were virtually identical. Autocorrelograms ($\pm$50 ms, 1-ms bin width), receptive field profiles (8 $\times$ 8°, 40-ms poststimulus), and orientation tuning curves (normalized to the peak firing rate) characteristic of the 3 neurons were the same at the 2 positions of the polytrode. Receptive fields were determined using binary m-sequence stimuli and reverse correlation (Jones and Palmer 1987); orientation tuning curves were derived from average ($n = 8$) responses to a drifting bar stimulus (0–360°, 20° increments).

(Buzsaki 2004; Churchland and Sejnowski 1992; Olshausen and Field 2004). Polytrodes are particularly well suited for this endeavor. No other currently available electrophysiological or imaging technique combines sub-millisecond temporal resolution with single-cell spatial resolution and the capability to sample neurons from a single extended volume of cortex (Campbell et al. 1991; Hoogerwerf and Wise 1994). The polytrodes described in this report are ideal for studies of columnar microcircuits because they enable exceptionally high-density recording of unit and field activity with minimal tissue damage. They give demonstrably better single-unit isolation than single electrodes, stereotrodes, or tetrodes and provide stable multiunit recordings for hours.

The finding that polytrodes with finer interconnects give robust recordings without increased noise or channel crosstalk augurs well for future polytrodes with even narrower conductors and spacing. The negligible crosstalk that was observed (<0.5%) for 1.5-μm feature sizes is in accord with predictions of an earlier theoretical study (Najafi et al. 1990) that concluded features could be scaled down to 1 μm with <1% crosstalk. Current industrial limits are in the submicrometer range, so even smaller high-density polytrodes should be realizable. Another potential concern was the viability of

neurons recorded by polytrodes with shank widths >60 μm, a problem that has been reported by other users of similar devices (Csicsvari et al. 2003). However, we did not observe any deterioration in the number or quality of units recorded across the entire shank having a width of ~200 μm (Fig. 2*B*). A narrower shank is nonetheless desirable for minimizing the cutting of axons and dendrites. As stated earlier, the main factor determining the overall shank width, and in turn the maximum number of recording sites on a single shank, is space for the interconnecting leads. Ultimately one-lead-per-site interconnects may become superfluous for polytrodes composed of active transistor arrays with on-chip multiplexing. Field effect transistor-based polytrodes with thousands of sites have already been prototyped for in vitro applications (Fromherz 2003). However, until serious complications involving the durability and high intrinsic noise of these devices are resolved, passive polytrodes with ≤1 μm feature sizes, narrower shank widths, and even more recording sites will continue to provide state-of-the-art high-density multiunit recordings. Other process variations, such as multilevel metal for the interconnect leads, offer the prospect of reducing the shank width of high-density passive arrays.

Two potential improvements to the current polytrode designs warrant mention. First penetration of the meninges could be aided by making the tip angle sharper (Najafi and Hetke 1990) or incorporating a silicon "spine" on the back of the shank to make it more rigid. The latter can be achieved by withdrawing the polytrode from the final etch before a complete etch-stop is achieved (Najafi et al. 1990) without increasing the overall width of the polytrode. We have also attempted to soften the dura and pia by partially digesting it with collagenase (Zhu et al. 2002), but this approach caused extensive spotted bleeding of the pial vasculature that we deemed more detrimental than a small incision at the point of penetration. Second, the recordings reported here were made with unmodified iridium recording sites. Controlled electrodeposition of gold can increase site surface area without increasing site diameter, reducing impedances by an order of magnitude (Blanche, unpublished observation). The lower input impedance of the sites in turn reduces the noise level. Optimizing the electrode-tissue interface by increasing the surface roughness and adhesive properties of the recording sites with synthetic polymers (Cui et al. 2003) is another avenue for enhancing recorded spike amplitudes. Either of these techniques could be adopted to improve the S:N of future recordings. If required, sites may also be modified for extracellular microstimulation after electrochemical "activation" to increase their charge capacity (Weiland and Anderson 2000).

Despite the huge datasets generated (aggregate bandwidth $\sim$2.8 MB/s; $\sim$10 GB/h), continuous acquisition has a number of benefits. It obviates the need to set trigger thresholds on-line, which is time consuming and impractical for polytrodes with more than a few sites. It eliminates the possibility of missing or duplicating spike events due to inappropriate window discriminator settings. The standard tetrode approach of recording an epoch from all channels in response to a threshold crossing is inappropriate for polytrodes extending over millimeters, and the usual method of "locking-out" the entire electrode array after a spike event makes detection of synchronous spikes impossible. In any case, there is little bandwidth to be saved by making episodic recordings considering the large numbers of active neurons typically recorded with polytrodes. Furthermore, because no data are lost at acquisition, as new and improved methods of spike sorting are developed it is possible to return to the archived files and re-extract spikes from the continuous waveforms.

The use of stereotrodes and tetrodes drew attention to the value of spatially sampling individual neurons, exploiting differential spike amplitudes on different sites to improve single-unit discrimination. High-density polytrodes take this idea to its logical conclusion by recording from most of each neuron's field potential. The result is a further improvement in the reliability of single neuron isolation. Given the disparity between the number of neurons per virtual tetrode we report and that usually cited for real wire-bundle tetrodes, the potential for mixed clusters in a highly active tetrode recording is probably worse than that suggested by the case study presented here (Fig. 3). The optimal sampling density and geometric configuration of recording sites needed to unambiguously resolve the activity of multiple neurons remains an open question. Each of the polytrode designs was, however, capable of recording individual neurons on multiple sites (Fig. 2H), so the question of "optimal" site spacing becomes more a question of specific

application. Due consideration should also be given to the brain region and species under study. Rat hippocampus, for example, is only $\sim$700 μm thick, but the limited spatial extent of interneuron field potentials in the dentate gyrus requires a polytrode with a site spacing ideally <50 μm (Freund and Buzsaki 1996). By way of contrast, only the two-column and one of the three-column polytrodes are long enough (>1.2 mm) to record simultaneously from all cortical layers of cat extrastriate visual cortex. In our present studies of the columnar circuits responsible for receptive field dynamics, translaminar coverage was particularly important, but a sampling resolution >50 μm is not justified. Finally, it should be noted that higher overall neuron yields might be obtained with multiple tetrodes because they can be independently moved to foci of high activity, but not with the high-density possible with single-shank polytrodes and at the expense of knowing the exact location of recorded units.

One of the challenges of recording from large numbers of sensory cortical neurons is devising appropriate stimuli, but it also presents an opportunity. A recent commentary by Olshausen and Field (2004) argues strongly that our incomplete understanding of sensory cortices is largely due to impoverished stimuli and biases in the design and execution of experiments. The usual paradigm for characterizing a single neuron by holding most stimulus dimensions constant and optimal, varying only the stimulus parameter of interest, is not only inherently biased (Towe 1973), but infeasible when recording from an assortment of neurons with a large range of optimal tuning responses. One solution is to present all combinations of relevant stimulus dimensions. Although time consuming, this has the benefit of impartial characterization of the neurons in the sample population, including those with small spike amplitudes or low firing rates that might otherwise have been overlooked. Time traditionally spent hunting for active neurons can instead be used to more fully characterize the response properties of the neuronal ensemble with a wide range of multi-dimensional stimuli, including natural scenes.

It is unrealistic to ascertain the exact location of cells recorded with standard tungsten and wire-bundle electrodes not only due to imprecision in histological track reconstruction, but because multiunit electrodes are potentially able to record from thousands of neurons within a $\sim$150-μm radius sphere, even further for large pyramidal neurons (Blanche et al. 2003; Buchwald et al. 1973; Fatt 1957; Henze et al. 2000; Rosenthal et al. 1966; Towe 1973). Knowledge of the spatial relations between recorded neurons is particularly important for receptive field mapping studies and, for example, in studies of cortical circuits where laminar position may be important. Questions surrounding the nature of cortical "micromaps," that is, whether the orderly arrangement of receptive field properties seen with optical imaging (Hubener et al. 1997) on the millimetric scale extends to the level of single cells on the microscale (Maldonado et al. 1997), motivated us to establish improved methods for localizing recorded neurons. Accurate positioning of the polytrode in the cortical layers (Figs. 5 and 6) is the first step. Capitalizing on the fixed site geometry and high resolution spike field potential measurements of the three column co-linear polytrode allowed us to refine the localization even further through development of a model-based approach to spatial neuron localization (Blanche et al. 2003; unpublished results). The algorithm is based on a mixed monopole-dipole

field model and is able to generalize to arbitrary neuron orientation, tissue anisotropies, and cell type. The shank of the polytrode acts as a ground plane, and therefore only neurons in front of the polytrode are recorded (Drake et al. 1988). If we also assume that the extracellular signal decay is isotropic along the two spatial dimensions co-planar with the cortical layers, then it is possible to estimate neuron locations in three dimensions with a two-dimensional electrode array. Polytrodes, when combined with precise neuron localization, are uniquely placed to resolve these outstanding physiological questions because they integrate high-density multiunit recording (microscale organization) with substantial coverage of whole cortical areas (millimetric scale organization). The neuron localization algorithm also enables polytrodes to track "constellations" of active neurons, the identification of which is unperturbed by electrode drift (Fig. 8). Combining spike shape information with the added constraint that the spatial relationships of the neurons do not change, provides a solid criteria for ensuring that the same neurons are being recorded from over periods of hours, days, or even months. This may prove particularly useful for chronic studies of the neural correlates of perceptual and motor learning (Gilbert et al. 2001; Paz et al. 2004), where long-term unambiguous identification of multiple neurons is critical.

Historically, extracellular electrodes do not provide any information about cell type—hence the terms unit and multiunit—nor anything about sub-threshold intracellular events. Broad classification of cell type into pyramidal and interneuron classes, currently the exclusive domain of intracellular recording (Nowak et al. 2003), can now be predicted by the neuron localization model on the basis of differences in field potential spread and asymmetry (Blanche et al. 2003), in addition to spike width (Bartho et al. 2004). This offers the prospect of explicitly studying the interactions between different neuronal classes thought to play specific roles in mechanisms of visual cortex tuning properties (Alonso and Martinez 1998; Hirsch et al. 2003). Finally, most of what is known about BPAPs and their possible role in spike-timing dependent plasticity (STDP) has come from in vitro work (Magee and Johnston 1997; Markram et al. 1997). Virtually no attention has been given to in vivo analyses of BPAPs, and only recently have in vivo reports of STDP begun to emerge (Fu et al. 2002; Yao and Dan 2001). Polytrodes offer the prospect of studying in vivo BPAPs (Fig. 2G), the brain state or behavioral conditions that evoke them, and their putative role as an associative signal in STDP.

APPENDIX

Site impedances were calculated by measuring the relative amplitude and phase lag of a 1-kHz, 10-mV_{rms} sinusoidal wave applied sequentially to each recording site. The circuit (Fig. A1) exploits voltage division of an AC signal across a reference resistor in series with a complex impedance to ground to determine the electrode site impedances

$$\vec{v} = \left(\frac{\bar{Z}}{\bar{Z} + R_{ref}}\right)\vec{v}_s \qquad (A1)$$

where $\bar{Z} = |Z|\angle\phi_Z$ is the amplitude and phase of the electrode site impedance, $\vec{v}^{\varpi} = |\bar{v}|\angle\phi_v$ is the amplitude and phase of the AC signal
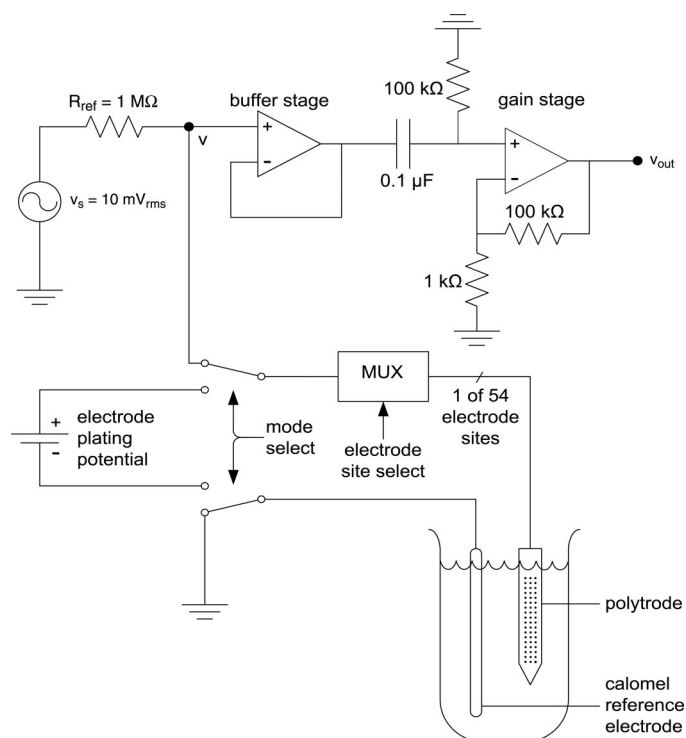

FIG. A1. Polytrode site impedance tester. Dual-purpose circuit for automated site impedance testing and electrode plating. TTL-level control lines on the DT3010 card switch the multiplexers and select the mode of operation via two relays (HE721C0500). A standard laboratory function generator, voltage divided to give a 10mV_{rms} AC test signal (v_s), is fed to individual electrode sites via a bank of analog multiplexers (MAX308). The resulting signal is buffered (LT1012C) and passed to a second op-amp where it is amplified 100x. The output signal (v_{out}) is digitized, along with the input signal, by one of the DT3010 acquisition cards used for multiunit recording. PC-based software uses both signals to calculate the site impedances according to equations (A2) and (A3) described in the APPENDIX.

measured across the site, $\vec{v}_s = |\vec{v}_s|\angle 0°$ is the sinusoidal source signal.

R_{ref} is a 1-MΩ reference resistor, roughly equal to the site impedance magnitude, making the voltage divider maximally sensitive to site impedance changes.

Solving for $|Z|$ and ϕ_Z gives

$$|Z| = \frac{|v|R_{ref}}{\sqrt{(|v_s| - |v|\cos\phi_v)^2 + (|v|\sin\phi_v)^2}} \qquad (A2)$$

$$\phi_z = \phi_v + \arctan\left(\frac{|v|\sin\phi_v}{|v_s| - |v|\cos\phi_v}\right) \qquad (A3)$$

Signal amplitudes and phases were obtained from fast Fourier transforms of the test signals (Press et al. 1994). *Equation A2* provides the impedance magnitude. The nature of the impedance (resistive or capacitive) is given by the phase angle from *Eq. A3*. To ensure sites are not damaged, extremely low test currents (<5 nA_{rms}) are applied. Faraday shielding and a low-noise op-amp yield a measurement precision of ±20 kΩ. The device also has an electroplating mode for electrodeposition of gold, a technique useful for lowering site impedances by increasing microscopic surface area. By switching rapidly and automatically between impedance and electroplating modes, it is possible to titrate the electrodeposition to achieve a desired impedance. Although not used in this paper, this part of the circuit has been retained for completeness. Additional details of the circuit, its construction, control software and calibration are available by contacting the authors.

REFERENCES

Alonso JM and Martinez LM. Functional connectivity between simple cells and complex cells in cat striate cortex. *Nat Neurosci* 1: 395–403, 1998.

Anderson DJ, Najafi K, Tanghe SJ, Evans DA, Levy KL, Hetke JF, Xue XL, Zappia JJ, and Wise KD. Batch-fabricated thin-film electrodes for stimulation of the central auditory system. *IEEE Trans Biomed Eng* 36: 693–704, 1989.

Bai Q and Wise KD. Single-unit neural recording with active microelectrode arrays. *IEEE Trans Biomed Eng* 48: 911–920, 2001.

Bartho P, Hirase H, Monconduit L, Zugaro M, Harris KD, and Buzsaki G. Characterization of neocortical principal cells and interneurons by network interactions and extracellular features. *J Neurophysiol* 92: 600–608, 2004.

Bierer JA and Middlebrooks JC. Auditory cortical images of cochlear-implant stimuli: dependence on electrode configuration. *J Neurophysiol* 87: 478–492, 2002.

Bishop PO, Burke W, and Davis R. The identification of single units in central visual pathways. *J Physiol* 162: 409–431, 1962a.

Bishop PO, Burke W, and Davis R. The interpretation of the extracellular response of single lateral geniculate cells. *J Physiol* 162: 451–472, 1962b.

Blanche TJ, Hetherington PA, Rennie CJ, Spacek MA, and Swindale NV. Model-based 3D cortical neuron localization and classification with silicon electrode arrays. *Soc Neurosci Abstr* 429.19, 2003.

Buchwald JS, Holstein SB, and Weber DS. Multiple unit recording: technique, interpretation, and experimental applications. In: *Bioelectric Recording Techniques*, edited by Thompson RF and Patterson MM. New York: Academic, 1973, p. 201–242.

Buzsaki G. Large-scale recording of neuronal ensembles. *Nat Neurosci* 7: 446–451, 2004.

Buzsaki G, Horvath Z, Urioste R, Hetke J, and Wise K. High-frequency network oscillation in the hippocampus. *Science* 256: 1025–1027, 1992.

Buzsaki G and Kandel A. Somadendritic backpropagation of action potentials in cortical pyramidal cells of the awake rat. *J Neurophysiol* 79: 1587–1591, 1998.

Campbell PK, Jones KE, Huber RJ, Horch KW, and Normann RA. A silicon-based, three-dimensional neural interface: manufacturing processes for an intracortical electrode array. *IEEE Trans Biomed Eng* 38: 758–768, 1991.

Chen J, Wise KD, Hetke JF, and Bledsoe SC Jr. A multichannel neural probe for selective chemical delivery at the cellular level. *IEEE Trans Biomed Eng* 44: 760–769, 1997.

Churchland PS and Sejnowski TJ. *The Computational brain.* Cambridge, MA: MIT Press, 1992.

Csicsvari J, Henze DA, Jamieson B, Harris KD, Sirota A, Bartho P, Wise KD, and Buzsaki G. Massively parallel recording of unit and local field potentials with silicon-based electrodes. *J Neurophysiol* 90: 1314–1323, 2003.

Cui X, Wiler J, Dzaman M, Altschuler RA, and Martin DC. In vivo studies of polypyrrole/peptide coated neural probes. *Biomaterials* 24: 777–787, 2003.

DiCarlo JJ, Lane JW, Hsiao SS, and Johnson KO. Marking microelectrode penetrations with fluorescent dyes. *J Neurosci Methods* 64: 75–81, 1996.

Drake KL, Wise KD, Farraye J, Anderson DJ, and BeMent SL. Performance of planar multisite microprobes in recording extracellular single-unit intracortical activity. *IEEE Trans Biomed Eng* 35: 719–732, 1988.

Ensell G, Banks DJ, Richards PR, Balachandran W, and Ewins DJ. Silicon-based microelectrodes for neurophysiology, micromachined from silicon-on-insulator wafers. *Med Biol Eng Comput* 38: 175–179, 2000.

Fatt P. Electric potentials occurring around a neuron during its antidromic activation. *J Neurophysiol* 20: 27–60, 1957.

Freund TF and Buzsaki G. Interneurons of the hippocampus. *Hippocampus* 6: 347–470, 1996.

Fromherz P. Neuroelectronic interfacing: semiconductor chips with ion channels, nerve cells, and brain. In: *Nanoelectronics and Information Technology*, edited by Waser R. Berlin: Wiley-VCH Verlag, 2003, p. 781–810.

Fu YX, Djupsund K, Gao H, Hayden B, Shen K, and Dan Y. Temporal specificity in the cortical plasticity of visual space representation. *Science* 296: 1999–2003, 2002.

Gilbert CD, Sigman M, and Crist RE. The neural basis of perceptual learning. *Neuron* 31: 681–697, 2001.

Gray CM, Maldonado PE, Wilson M, and McNaughton B. Tetrodes markedly improve the reliability and yield of multiple single-unit isolation from multi-unit recordings in cat striate cortex. *J Neurosci Methods* 63: 43–54, 1995.

Harris KD, Henze DA, Csicsvari J, Hirase H, and Buzsaki G. Accuracy of tetrode spike separation as determined by simultaneous intracellular and extracellular measurements. *J Neurophysiol* 84: 401–414, 2000.

Henze DA, Borhegyi Z, Csicsvari J, Mamiya A, Harris KD, and Buzsaki G. Intracellular features predicted by extracellular recordings in the hippocampus in vivo. *J Neurophysiol* 84: 390–400, 2000.

Hetherington PA, Blanche TJ, and Swindale NV. Prediction of neuron 3D cortical location by triangulation of spike signals from silicon electrode recording arrays. *Soc Neurosci Abstr* 25, 1422, 1999.

Hetherington PA and Swindale NV. Receptive field and orientation scatter studied by tetrode recordings in cat area 17. *Vis Neurosci* 16: 637–652, 1999.

Hetke JF, Lund JL, Najafi K, Wise KD, and Anderson DJ. Silicon ribbon cables for chronically implantable microelectrode arrays. *IEEE Trans Biomed Eng* 41: 314–321, 1994.

Hirsch JA, Martinez LM, Pillai C, Alonso JM, Wang Q, and Sommer FT. Functionally distinct inhibitory neurons at the first stage of visual cortical processing. *Nat Neurosci* 6: 1300–1308, 2003.

Hoogerwerf AC and Wise KD. A three-dimensional microelectrode array for chronic neural recording. *IEEE Trans Biomed Eng* 41: 1136–1146, 1994.

Hubener M, Shoham D, Grinvald A, and Bonhoeffer T. Spatial relationships among three columnar systems in cat area 17. *J Neurosci* 17: 9270–9284, 1997.

Humphrey DR. Neural networks and systems modeling. In: *Biological foundations of Biomedical Engineering*, edited by Kline J. Boston, MA: Little, Brown, 1976.

Jog M, Connolly C, Kubota Y, Iyengarm D, Garrido L, Harlan R, and Graybiel A. Tetrode technology: advances in implantable hardware, neuroimaging, and data analysis techniques. *J Neurosci Methods* 117: 141–152, 2002.

Johnston D, Magee JC, Colbert CM, and Cristie BR. Active properties of neuronal dendrites. *Annu Rev Neurosci* 19: 165–186, 1996.

Jones JP and Palmer LA. The two-dimensional spatial structure of simple receptive fields in cat striate cortex. *J Neurophysiol* 58: 1187–1211, 1987.

Kandel A and Buzsaki G. Cellular-synaptic generation of sleep spindles, spike-and-wave discharges, and evoked thalamocortical responses in the neocortex of the rat. *J Neurosci* 17: 6783–6797, 1997.

Kewley DT, Hills MD, Borkholder DA, Opris IE, Maluf NI, Storment CW, Bower JM, and Kovacs GT. Plasma-etched neural probes. *Sensors and Actuators A: Phys A* 58: 27–35, 1997.

Kovacs GT, Storment CW, Halks-Miller M, Belczynski CR, Jr, Della Santina CC, Lewis ER, and Maluf NI. Silicon-substrate microelectrode arrays for parallel recording of neural activity in peripheral and cranial nerves. *IEEE Trans Biomed Eng* 41: 567–577, 1994.

Magee JC and Johnston D. A synaptically controlled, associative signal for Hebbian plasticity in hippocampal neurons. *Science* 275: 209–213, 1997.

Mahalanobis PC. On the generalized distance in statistics. *Proc Natl Inst Sci India* 2: 49–55, 1936.

Maldonado PE, Godecke I, Gray CM, and Bonhoeffer T. Orientation selectivity in pinwheel centers in cat striate cortex. *Science* 276: 1551–1555, 1997.

Maldonado PE and Gray CM. Heterogeneity in local distributions of orientation-selective neurons in the cat primary visual cortex. *Vis Neurosci* 13: 509–516, 1996.

Markram H, Lubke J, Frotscher M, and Sakmann B. Regulation of synaptic efficacy by coincidence of postsynaptic APs and EPSPs. *Science* 275: 213–215, 1997.

McNaughton BL, O'Keefe J, and Barnes CA. The stereotrode: a new technique for simultaneous isolation of several single units in the central nervous system from multiple unit records. *J Neurosci Methods* 8: 391–397, 1983.

Mensinger AF, Anderson DJ, Buchko CJ, Johnson MA, Martin DC, Tresco PA, Silver RB, and Highstein SM. Chronic recording of regenerating VIIIth nerve axons with a sieve electrode. *J Neurophysiol* 83: 611–615, 2000.

Mitzdorf U. Current source-density method and application in cat cerebral cortex: investigation of evoked potentials and EEG phenomena. *Physiol Rev* 65: 37–100, 1985.

Mitzdorf U and Singer W. Prominent excitatory pathways in the cat visual cortex (A 17 and A 18): a current source density analysis of electrically evoked potentials. *Exp Brain Res* 33: 371–394, 1978.

Najafi K and Hetke JF. Strength characterization of silicon microprobes in neurophysiological tissues. *IEEE Trans Biomed Eng* 37: 474–481, 1990.

Najafi K, Ji J, and Wise KD. Scaling limitations of silicon multichannel recording probes. *IEEE Trans Biomed Eng* 37: 1–11, 1990.

Najafi K, Wise K, and Mochizuki T. A high-yield ic-compatible multichannel recording array. *IEEE Trans Electron Devices* 32: 1206–1211, 1985.

Najafi K and Wise KD. An implantable multielectrode array with on-chip signal processing. *IEEE J Solid-State Circuits* 21: 1035–1044, 1986.

Nicholson C and Freeman JA. Theory of current source-density analysis and determination of conductivity tensor for anuran cerebellum. *J Neurophysiol* 38: 356–368, 1975.

Niparko JK, Altschuler RA, Xue XL, Wiler JA, and Anderson DJ. Surgical implantation and biocompatibility of central nervous system auditory prostheses. *Ann Otol Rhinol Laryngol* 98: 965–970, 1989.

Norlin P, Kindlundh M, Mouroux A, Yoshida K, and Hofmann UG. A 32-site neural recording probe fabricated by DRIE of SOI substrates. *J Micromech Microeng* 12: 414–419, 2002.

Nowak LG, Azouz R, Sanchez-Vives MV, Gray CM, and McCormick DA. Electrophysiological classes of cat primary visual cortical neurons in vivo as revealed by quantitative analyses. *J Neurophysiol* 89: 1541–1566, 2003.

Olshausen BA and Field DJ. What is the other 85% of V1 doing? In: *Problems in Systems Neuroscience*, edited by Sejnowski TJ and van Hemmen L. Oxford, UK: Oxford Univ. Press. 2005 In press.

Paz R, Wise SP, and Vaadia E. Viewing and doing: similar cortical mechanisms for perceptual and motor learning. *Trends Neurosci* 27: 496–503, 2004.

Press WH, Teukolsky SA, Vetterling WT, and Flannery BP. *Numerical Recipes in Fortran 77: The Art of Scientific Computing.* Cambridge, MA: Cambridge, 1994.

Rathnasingham R, Kipke DR, Bledsoe SC, Jr, and McLaren JD. Characterization of implantable microfabricated fluid delivery devices. *IEEE Trans Biomed Eng* 51: 138–145, 2004.

Rosenthal F, Woodbury JW, and Patton HD. Dipole characteristics of pyramidal cell activity in cat postcruciate cortex. *J Neurophysiol* 29: 612–625, 1966.

Rousche PJ and Normann RA. Chronic recording capability of the Utah Intracortical Electrode Array in cat sensory cortex. *J Neurosci Methods* 82: 1–15, 1998.

Rousche PJ and Normann RA. Chronic intracortical microstimulation (ICMS) of cat sensory cortex using the Utah Intracortical Electrode Array. *IEEE Trans Rehabil Eng* 7: 56–68, 1999.

Spacek MA, Blanche TJ, Douglas RM, and Swindale NV. Signal processing and spike detection methods for high-density silicon electrode arrays. *Soc Neurosci Abstr* 429.20, 2003.

Spence AJ, Hoy RR, and Isaacson MS. A micromachined silicon multielectrode for multiunit recording. *J Neurosci Methods* 126: 119–126, 2003.

Starr A, Wise K, and Csongradi J. An evaluation of photoengraved microelectrodes for extracellular single-unit recording. *IEEE Trans Biomed Eng* 20: 291–293, 1973.

Takahashi K and Matsuo T. Integration of multi-microelectrode and interface circuits by silicon planar and three-dimensional fabrication technology. *Sensors Actuators* 5: 89–99, 1984.

Towe AL. Sampling Single Neuron Activity. In: *Bioelectric Recording Techniques*, edited by Thompson RF and Patterson MM. New York: Academic, 1973, p. 79–93.

Vetter RJ, Williams JC, Hetke JF, Nunamaker EA, and Kipke DR. Chronic neural recording using silicon-substrate microelectrode arrays implanted in cerebral cortex. *IEEE Trans Biomed Eng* 51: 896–904, 2004.

Vornov JJ, Tasker RC, and Coyle JT. Direct observation of the agonist-specific regional vulnerability to glutamate, NMDA, and kainate neurotoxicity in organotypic hippocampal cultures. *Exp Neurol* 114: 11–22, 1991.

Weiland JD and Anderson DJ. Chronic neural stimulation with thin-film, iridium oxide electrodes. *IEEE Trans Biomed Eng* 47: 911–918, 2000.

Wilson MA and McNaughton BL. Dynamics of the hippocampal ensemble code for space. *Science* 261: 1055–1058, 1993.

Wise KD and Najafi K. Microfabrication techniques for integrated sensors and microsystems. *Science* 254: 1335–1342, 1991.

Yao H and Dan Y. Stimulus timing-dependent plasticity in cortical processing of orientation. *Neuron* 32: 315–323, 2001.

Yoon TH, Hwang EJ, Shin DY, Park SI, Oh SJ, Jung SC, Shin HC, and Kim SJ. A micromachined silicon depth probe for multichannel neural recording. *IEEE Trans Biomed Eng* 47: 1082–1087, 2000.

Zhu Z, Wang Y, Xu XZ, and Li CY. A simple and effective method for obtaining stable in vivo whole-cell recordings from visual cortical neurons. *Cereb Cortex* 12: 585–589, 2002.